Mon. Not. R. Astron. Soc. **000**, 1–**??** (2009)   Printed 16 November 2009   (MN LaTeX style file v2.2)

arXiv:0911.2711v1 [astro-ph.HE] 13 Nov 2009

X-ray observations of SU UMa throughout six outbursts

David J. Collins⋆ and Peter J. Wheatley†
Department of Physics, University of Warwick, Coventry CV4 7AL, UK

16 November 2009

ABSTRACT

We present *RXTE* observations covering six normal outbursts of the dwarf nova SU UMa, the prototype of its class. The outbursts showed consistent X-ray behaviour with the X-ray count rate dropping suddenly by a factor of four, and with evidence for a half day delay between the optical rise and the X-ray suppression. In contrast to SS Cygni, an X-ray flux increase at the beginning of outburst was not observed, although it is expected from boundary layer models. The X-ray flux was high and decreasing during quiescence, in conflict with the disc instability model. The X-ray spectrum of SU UMa was softer in outburst than during quiescence, and it was consistent with constant reflection.

Key words: Accretion, accretions disks - Binaries: close - Stars: novae, cataclysmic variables - Stars: individual: SU UMa - X-rays: stars

1 INTRODUCTION

Cataclysmic variables are close binary systems in which a red dwarf secondary star transfers mass via Roche lobe overflow to a white dwarf primary (see Warner (1995) for a review). Material is accreted by the white dwarf through an accretion disc and in dwarf novae the disc is unstable and undergoes regular outbursts. SU UMa-types are a subclass of dwarf novae which exhibit two types of outbursts: normal outbursts and superoutbursts. Superoutbursts occur less frequently, last longer and are brighter than normal outbursts.

In the standard model about half of the gravitational energy of the accreting matter is released in a boundary layer between the accretion disc and the white dwarf (Shakura & Syunyaev 1973; Pringle 1977; Tylenda 1981). This energy is thought to be emitted as X-rays due to shock heating as the accreting material settles on to the white dwarf surface. Therefore X-ray observations are sensitive to the mass transfer rate through the accretion disc and to conditions in the inner accretion disc.

Dwarf novae are sources of hard X-rays in quiescence and observations of eclipsing systems support the boundary layer model demonstrating that the X-rays arise in the immediate vicinity of the white dwarf, at least in quiescence (e.g. Mukai et al. 1997; Wheatley & West 2003).

The X-ray spectrum in quiescence is a hot optically thin plasma (e.g. Eracleous et al. 1991). Observed lines indicate that the X-ray emitting plasma covers a wide range of temperatures (e.g. Baskill et al. 2005) and is consistent with a cooling plasma settling onto the white dwarf through a disc boundary layer (e.g. Wheatley et al. 1996; Pandel et al. 2005).

In outburst the hard X-rays are usually suppressed and replaced with an intense extreme ultraviolet component (e.g. Wheatley et al. 2003). This is thought to be due to the boundary layer becoming optically thick to its own emission as the accretion rate increases during outburst (Pringle & Savonije 1979; Patterson & Raymond 1985). However, the X-ray flux evolution through the outburst cycle is not well reproduced by the standard disc instability model (e.g. Lasota 2001).

Most X-ray observations are too short to follow the flux evolution through outburst, and our observational picture is still based on just a handful of well studied outbursts: SS Cygni (Ricketts et al. 1979; Jones & Watson 1992; Wheatley et al. 2003), VW Hyi (Pringle et al. 1987; Wheatley et al. 1996), YZ Cnc (Verbunt et al. 1999), WZ Sge (Wheatley & Mauche 2005). In some cases systems have been seen to deviate from the standard picture (e.g. U Gem, Cordova & Mason 1984; GW Lib, Byckling et al. 2009), but it is not clear whether individual systems exhibit a range of behaviour or whether each system exhibits consistent behaviour.

In this paper we present X-ray observations spanning six outbursts of the dwarf nova SU UMa. Snapshot observations have shown that in quiescence SU UMa is a source of hard X-rays, emitted from a hot optically thin boundary layer region (Eracleous et al. 1991). In outburst the count rate has been seen to drop by a factor of 3 (Silber et al. 1994). High resolution data taken with the *Chandra HETG* during quiescence showed the presence of a weak fluorescent iron line indicating there may be reflection present in the system (Rana et al. 2006).

By monitoring a system throughout multiple outbursts, we aim to determine whether the X-ray flux evolution is consistent between different outburst cycles.

⋆ E-mail: D.J.Collins@warwick.ac.uk
† E-mail: P.J.Wheatley@warwick.ac.uk

2 OBSERVATIONS

SU UMa was monitored using the *RXTE* Proportional Counter Array (*PCA*) beginning on 2001 March 25 and ended on 2001 June 21. The observations spanned six normal outbursts. The total exposure was 336 ks observed over 193 visits taken in blocks of 1 – 14 ks exposure with gaps due to Earth occultations and passage of the spacecraft through the South Atlantic Anomaly (SAA). All *RXTE* count rates in this paper are for three *PCU*s.

The data were extracted using `FTOOLS`, version 6.1.2, provided by the High Energy Astrophysics Science Archive Research Centre.[1] Only the top xenon layer was used and the *PCA* data were extracted in Standard-2 binned mode. `saextrct`, version 4.2e, was used to produce light curves with a time resolution of 16 seconds, and spectral files binned into 129 channels. Data were excluded where the elevation was less than 10 degrees, the ELECTRON2 ratio was greater than 0.1 and the time since SAA passage was under 10 minutes. On 2000 May 13 *PCU*0 suffered a loss of propane from its veto layer resulting in a higher number of false events being observed in that detector. As a result this detector was not used in the extraction of the data set. `pcabackest`, version 3.0 and `pcarsp`, version 10.1, were used to calculate the background, and response matrix. Data from different detector configurations were extracted as separate spectra an re-binned using `rbnpha`, version 2.1.0.

3 TIME SERIES ANALYSIS

The *RXTE* observations cover six normal outbursts of SU UMa. Figure 1 shows the X-ray observations plotted with optical observations from the *AAVSO*. The optical data consist of visual observations (85 per cent) and V band CCD observations (15 per cent) with an average cadence of 5 hours (but usually concentrated into night time in the USA). In outburst the optical band rapidly brightened from approximately 14^{th} to 12^{th} mag in approximately 0.5 days before declining back into quiescence. Outbursts were nearly equally spaced, lasting approximately 2 days with the quiescence periods lasting approximately 10 days.

In the hard X-ray band as the system enters outburst the X-rays become suppressed to near zero. The X-ray flux remains suppressed for most of the duration of the outburst, recovering during optical decline. The beginning of each outburst is shown in more detail in Fig. 2, and there is no sign of a peak preceeding the X-ray suppression, as was observed in SS Cygni. The cadence of X-ray observations at the beginning of the outbursts was typically 12 hours.

Also plotted in Fig. 1 is the X-ray hardness ratio which was created using counts in the energy bands 2.0−3.7 keV and 3.7−18.5 keV. During quiescence the hardness ratio does not show any obvious variations, although at JD 2452012 for approximately 4 days a higher X-ray count rate was accompanied by a harder spectrum. Despite large error bars during outburst it is clear that the system is softer during outburst than during quiescence . This has also been seen in other dwarf novae (e.g. Baskill et al. 2005). Closer inspection of Fig. 1 shows that the softening of the spectrum coincides with the hard X-rays becoming quenched.

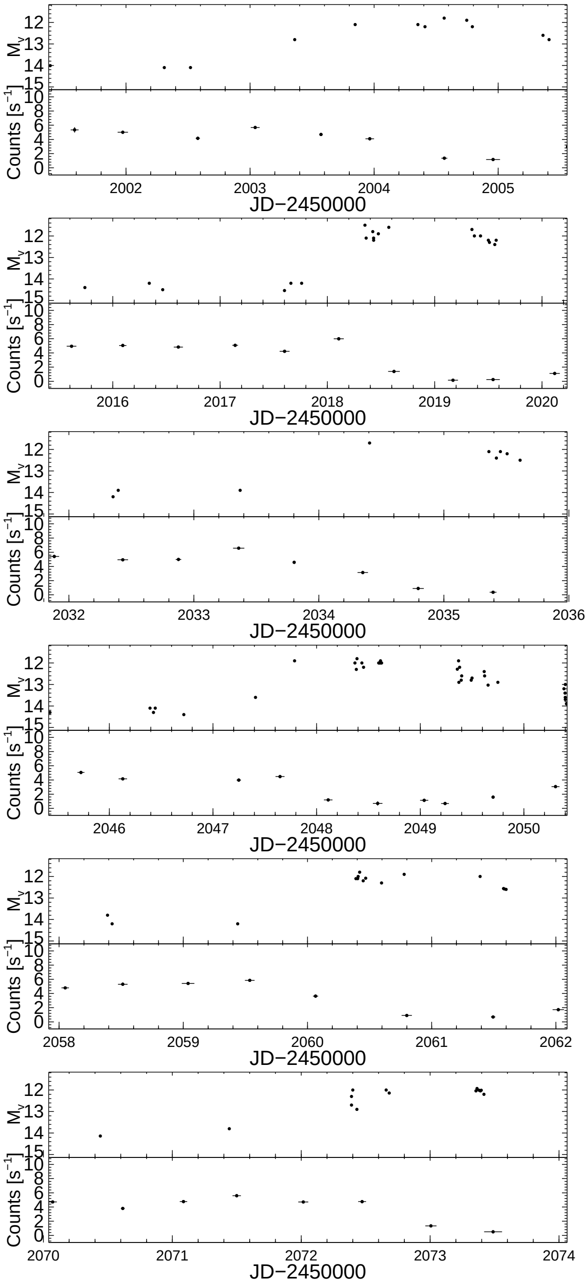

Figure 2. Detailed sections of the optical (upper panel) and X-ray (bottom panel) light curves from Fig. 1 during the transition to outburst. The X-ray count rates are for 3 *PCU*.

To make comparison between the outbursts a composite light curve was made of the six outbursts, Fig. 3. The times were shifted to maximise the auto-correlation in the optical band using the second outburst as a template (JD 2452017). The composite light curve shows that the shapes of the six outbursts were highly repeatable. In both the optical and X-ray bands the quiescent periods following outburst were more variable than prior to the outbursts. A peak in the count rate immediately before outburst was also not observed in the composite light curve, which has an average separation of points of only 2 hours. The X-ray suppression is remarkably rapid

---

[1] http://heasarc.gsfc.nasa.gov/ftools

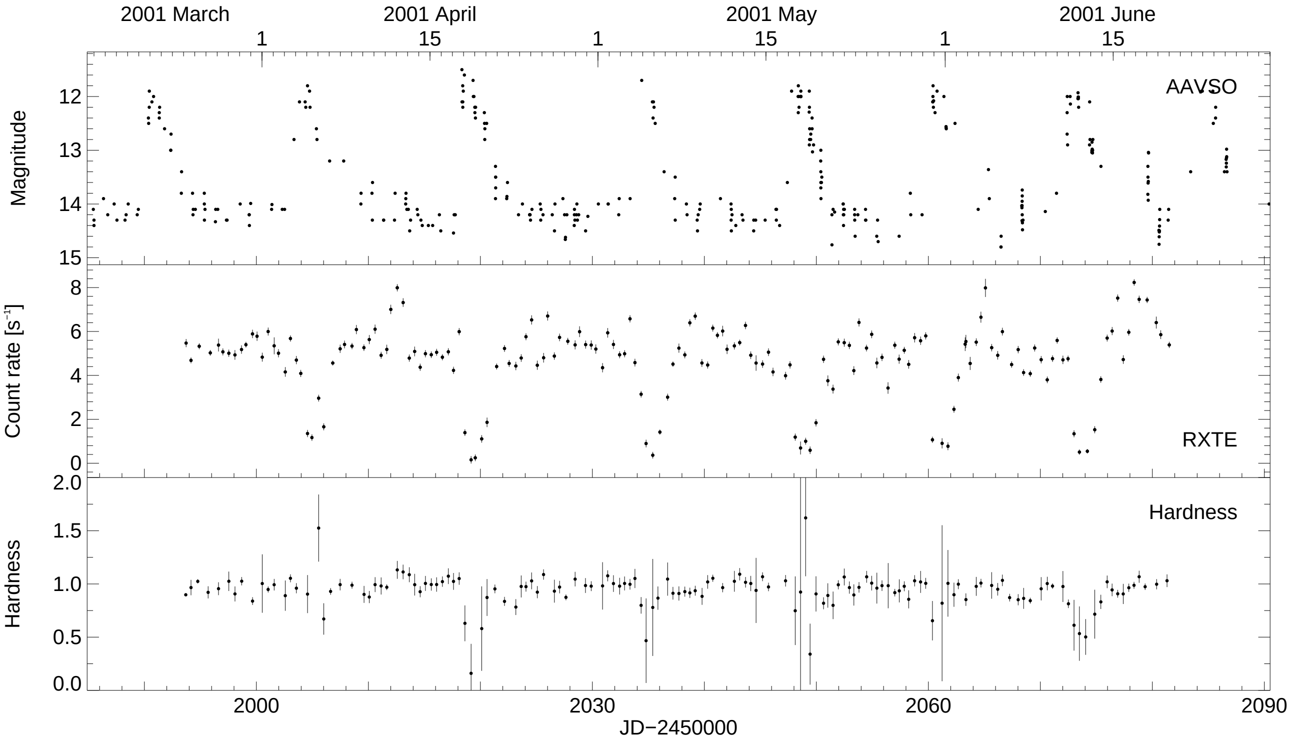

Figure 1. *AAVSO* (upper panel) and *RXTE* (middle panel) observations of SU UMa during the March - June 2001. The X-ray hardness ratio, defined as the hard band, 3.7 – 18.5 keV, divided by the soft band, 2.0 – 3.7 keV, is also plotted. The X-ray count rates are for 3 *PCU*.

Table 1. Optical and X-ray times for the flux to reach mid-point of the transition to outburst, including the cadence of the optical and X-ray observations respectively.

Optical time [JD]	Cadence [days]	X-ray time [JD]	Cadence [days]	Delay [days]
2452003.0	0.79	2452004.1	0.60	1.12
2452017.9	0.47	2452018.4	0.46	0.45
2452033.6	1.03	2452034.3	0.42	0.68
2452047.5	0.39	2452047.8	0.42	0.34
2452059.8	0.88	2452060.1	0.68	0.25
2452071.8	0.88	2452072.7	0.47	0.86

and is not resolved in the composite light curve, suggesting it occurs faster than two hours.

Figure 3 also shows there is a delay between the start of outburst in the optical and X-ray bands, however, due to the sparse sampling of both optical and X-ray data it is difficult to determine the precise duration of the delay. To quantify the delay the data were interpolated and times when the X-ray and optical flux crossed the mid point between outburst and quiescence were calculated, these times are shown in Table 1. The delays show that the X-ray suppression follows the optical rise by 0.25 – 1.12 days later, with a median delay of 0.57 days. The range in delay times can be accounted for by the cadence of the observations (also listed in Table 1).

In order to determine whether the X-ray flux increases during quiescence, as predicted by the disc instability model, we performed a linear least squares fit to the quiescent intervals, plotted in Fig. 4. The X-ray observations were selected when the optical light curve was fainter than 14th mag. There is short timescale variability in the light curves, but the quiescent trend is well represented by the best fit lines. The fits show that the quiescent X-ray count rate either remains constant or decreases. The gradients of the line fits are presented in Table 2. Figure 5 shows the composite light curve of Fig. 4 with a linear least squares fit to the all the quiescent data. The fit was applied to the interval where the optical was fainter than 14th mag in all six cycles. It shows that, in addition to short timescale variability, there is an overall decline in the hard X-ray flux during quiescence. The mean count rate decreased from a maximum of 5.8 counts s^{-1}, with a gradient of 0.09 counts s^{-1} day^{-1}, although the average decline is not well represented by a straight line (χ^2_ν = 4.9 with 5 degrees of freedom). A similar decline during quiescence has previously been seen in SS Cygni by McGowan et al. (2004).

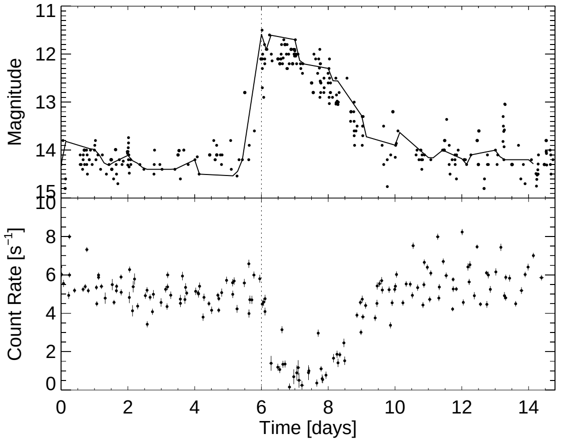

Figure 3. The *AAVSO* (upper panel) and *RXTE* (bottom panel) outbursts from Fig. 1 auto correlated and overlaid. The second optical outburst (thick line) was used as the template. The X-ray count rates are for 3 *PCU*.

Table 2. Gradients for the linear least squares fits to the quiescent X-ray data from Fig 4 and Fig 5.

Quiescence interval [JD]	Gradient [counts s^{-1} $days^{-1}$]
2451999	$+0.01 \pm 0.02$
2452013	-0.22 ± 0.02
2452028	$+0.00 \pm 0.01$
2452042	-0.14 ± 0.02
2452055	$+0.06 \pm 0.02$
2452068	-0.38 ± 0.03
Composite	-0.09 ± 0.02

4 SPECTRAL FITTING

4.1 Combined quiescence spectrum

The data were initially binned into one quiescent spectrum containing data with count rates higher than 3 $counts^{-1}$ (per 3 *PCU*s), resulting in a total exposure of 251 ks. We adopted a systematic error of 0.5 per cent (e.g. Wilms et al. 1999; Jahoda et al. 2006; Wilms et al. 2006) applied to the background subtracted data. Since SU UMa is faint the systematic uncertainty in the background is likely to contribute significantly, this will be addressed in more detail in Section 4.2. The data were initially fitted with the error on the background set to zero.

A single temperature thermal plasma model was fitted to the data; the mekal model in `XSPEC` (Mewe et al. 1985, 1986; Liedahl et al. 1995). Applying this model to the quiescent spectrum did not result in a good fit with a χ^2_ν of 13 (36 d.o.f). The residuals, Fig. 6 panel A, show that there is an excess in the model between 6 – 8 keV. Comparing the plotted model and data it is apparent that this excess comes from the modelled iron line emission in the thermal plasma model. Reducing the strength of the thermal lines can be achieved by lowering the metal abundances. Making the model abundances a free parameter gave a significant improvement to the fit resulting in a χ^2_ν of 3.6 (35 d.o.f) with an ftest probability of 2×10^{-11}. The residuals to this model can be seen in Fig. 6 panel B. The best fit abundances were found to be lower than solar levels (Anders & Grevesse 1989) at 0.64 ± 0.01 solar. Sub-solar abundances have been found for other dwarf novae (e.g. Baskill et al. 2005).

The modification to the model reduced the size of the excess in the residuals (Fig. 6 panel B) but it was still poorly fitting in the 6 − 8 keV energy range. The residuals show a deficit in the model between 6 − 7 keV providing evidence for a 6.4 keV fluorescence line of neutral iron, also seen in SU UMa by Rana et al. (2006). A narrow Gaussian component fixed at 6.4 keV was added to the model, and the result of this addition is seen in Fig. 6 panel C. The fit produces a χ^2_ν of 2.01 (34 d.o.f). The addition of the narrow emission line improved the fit between 6 – 8 keV, but it was unable to remove the residual feature near 7 keV.

4.2 Background systematics

The unacceptably high χ^2_ν produced by these fits indicates that either the model is inadequate, or systematic uncertainties are present in the data that are not fit by the model. Extensive analysis of the calibration and background model for the *PCA* was carried out by Jahoda et al. (2006). They determined that the energy calibration has deviations of $\leqslant$ 1 per cent from power law fits to the Crab Nebula and unmodeled variations in the instrumental background at $\leqslant$ 2 per cent below 10 keV and $\leqslant$ 1 per cent between 10 − 20 keV. When `saextrct` generates the data files the error is calculated as the square root of the number of counts in the data file. This is correct for the data, however, the background is estimated from the average of a huge amount of data and so the resulting error on the background is overestimated.[2] A value of zero was used as the background error in the fitting in Section 4.1. However, SU UMa is a faint system, so background systematics are likely to contribute significantly.

To investigate the level of systematic error required on the background, the data were re-binned forming eight spectra. Using the same criteria as above, observations with count rates lower than 3 $counts^{-1}$ (per 3 *PCU*s), based on Fig. 1, were considered to be in outburst and were binned into one outburst spectrum containing 48 ks of exposure. One spectrum was made for each quiescent period between the outbursts with each quiescent spectrum containing an average of 36 ks of exposure. A systematic error of 0.5 per cent was applied to the background subtracted spectrum as before, and a histogram of the χ^2_ν distribution was produced from the model fits. A series of fits were made with the systematic error on the background selected in the range 0 − 1 per cent, as identified by Jahoda et al. (2006). The data were fitted using the current best model: a thermal plasma model with free abundances and a narrow emission line fixed at 6.4 keV. Figure 7 shows the cumulative histogram plots of the best fit χ^2_ν distributions, with the cumulative plot of the χ^2 distribution (curve) on the same plot. The plots show that a systematic error of 0 and 0.1 per cent in the background underestimates the error resulting in distributions that are greater than 1. Similarly a systematic error of between 0.8 and 1 per cent overestimate the error and result in distributions that are less than 1. A systematic error between 0.3 and 0.5 per cent produces a distribution that is closest to a χ^2 distribution, with a background systematic error of 0.5 per cent producing the best result. Since this is within the range identified by Jahoda et al. (2006) and produced acceptable fits to the model, this value was adopted and applied to all data.

Fitting the quiescent and outburst spectra with the new background systematic error resulted in an acceptable χ^2_ν for all spectra. We also found an acceptable fit with a χ^2_ν of 0.99 (34 d.o.f) to the combined quiescent spectrum in Section 4.1.

4.3 Time resolved spectra

The best fit parameters resulting from the fit to the thermal plasma model with narrow emission line are shown in Fig. 8. The flux of the quiescent spectra varies during the observation with the seventh spectrum emitting more X-rays on average than the other quiescent spectra. The system is also fainter and softer in outburst than in quiescence. Within error the temperature of the quiescent spectra are consistent with each other at an average temperature of 7.8 ± 0.3 keV. The outburst spectrum fitted a lower temperature of 3.8 ± 0.4 keV. The best fit free abundances were also consistent with each other producing an average abundance of 0.64 ± 0.01 solar. The outburst spectrum was less well constrained fitting an abundance of 0.62 ± 0.25, however it is still consistent with the quiescent spectra. The 6.4 keV line strength is weaker in the earlier quiescent intervals, but within the error all spectra are consistent with each other, with an average equivalent width of 91 ± 35 eV during quiescence. The best fit line strength during outburst is consistent with the quiescent spectrum but is poorly constrained (102 ± 102 eV). These equivalent widths are also consistent with equivalent widths expected from a semi-infinite, plane parallel cold slab irradiated by an external source of X-rays (George & Fabian 1991). Fitting a fixed reflection continuum (calculated from the code of Magdziarz & Zdziarski 1995), with the reflector abundances tied to the abundances of the plasma model, does not improve the best fit. However, it does show that the data are consistent with a reflection continuum with a total best fit χ^2_ν of 1.3 (251 d.o.f).

---

[2] http://astrophysics.gsfc.nasa.gov/xrays/programs/rxte/pca/chisquare.html

It is possible to investigate the reflection in the system based on the fluorescent line and flux above 7 keV, since only photons above 7 keV have enough energy to be able to produce fluorescence photons that contribute to the 6.4 keV emission line. The line normalisation and the line flux above 7 keV are plotted in Fig. 9 which shows the fraction of continuum photons that produce line photons. If the amount of reflection in the system is constant then as the continuum emission increases the line emission will also increase. Thus a straight line is expected, with the gradient of the best fit line in Fig. 9 representative of the reflection in the system. As the flux from the X-ray source decreases the number of photons producing fluorescence line photons also decreases, thus the best fit line is expected to have an intercept that passes near to zero. The figure shows there is a good correlation with the flux between 7 – 20 keV and the line normalisation. The gradient of the line shows that ~ 4 per cent of hard X-rays give rise to fluorescent photons. The linear fit is consistent with no change in reflection during these observations.

4.4 Multi-temperature fits

The X-ray spectrum originates from an optically thin plasma that probably consists of a wide range of temperatures, previously modelled as a cooling flow (Wheatley et al. 1996; Pandel et al. 2005). We attempted to fit a multi-temperature model to the combined quiescent spectrum (cemekl in `XSPEC`, Singh et al. 1996) which showed that $\alpha \geqslant 0.8$, $T_{max} = 12^{+2}_{-4}$ keV and abundance = 0.59 ± 0.05 with a χ^2_ν of 0.97 (33 d.o.f) confirming low abundances. T_{max} and α are consistent with *ASCA* observations of other dwarf novae in quiescence (Baskill et al. 2005).

4.5 Fluxes and luminosity

Fluxes were calculated from the best fitting model over the energy range 2 – 20 keV. Broad band fluxes were calculated by integrating over the energy range 0.01 – 100 keV. They are presented in Table 3 along with the luminosities and associated accretion rates. Assuming a distance of 260^{+190}_{-90} pc to SU UMa (Thorstensen 2003) the average X-ray luminosity of the system was calculated to be $2.6{\times}10^{32}(d/260pc)^2$ erg s^{-1} in quiescence and $0.7{\times}10^{32}(d/260pc)^2$ erg s^{-1} in outburst. We note that although the outburst flux is consistent with that calculated by Baskill et al. (2005) it is close to the confusion limit of the *RXTE* detector (Jahoda et al. 2006). The accretion rates were calculated using the relation $L = GM_{wd}\dot{M}/2R_{wd}$. The mass of the white dwarf in SU UMa has not been directly calculated owing to its low inclination. Based on the work of Knigge (2006) white dwarfs in binaries were found to have an average mass of $M_{wd} = 0.75M_\odot$ and $R_{wd} = 7.7 \times 10^8$ cm. These values were used to calculate the accretion rates presented here. The calculated luminosities correspond to an average accretion rate during quiescence of 4.2×10^{15} g s^{-1} and 1.2×10^{15} g s^{-1} during outburst. However, the accretion rate is not thought to drop during outburst, instead the luminosity is probably dominated by an intense extreme ultraviolet component.

Table 3. Fluxes, luminosities and associated accretion rates for SU UMa.

Time	Flux^a		Luminosity^b	Accretion rate^c
[JD]	2 – 20 keV	0.01 – 100 keV		
2451999	1.7	2.8	2.3	3.8
2452013	1.9	3.2	2.6	4.3
2452028	1.8	3.0	2.4	4.0
2452042	1.8	3.1	2.5	4.1
2452055	1.9	3.2	2.6	4.2
2452068	1.8	3.0	2.4	4.0
2452079	2.3	3.9	3.1	5.2
Outburst	0.4	0.9	0.7	1.2

^{a} $\times 10^{-11}$ ergs s^{-1} cm^{-2}
^{b} $\times 10^{32}(d/260pc)^2$ ergs s^{-1}
^{c} $\times 10^{15}$ g s^{-1}

5 DISCUSSION AND CONCLUSIONS

We have presented X-ray observations of SU UMa spanning six normal outbursts. We have studied the X-ray flux evolution of SU UMa in much greater detail than has been possible with the brief snapshot observations that previous analysis has relied on.

All six outbursts showed consistent X-ray behaviour. At the start of outburst the X-rays were suddenly quenched to near zero, the X-ray count rate dropping by nearly a factor of 4. This is consistent with snapshot observations by Silber et al. (1994) who measured the *ROSAT* X-ray count rate to be a factor of 3 lower in outburst. A larger drop in X-rays is measured from *RXTE* data since the spectrum gets softer as well as fainter. Observation of VW Hyi, also a SU UMa type variable, showed the flux to drop by a factor of 6 (Wheatley et al. 1996).

Calculating times for the optical and X-ray fluxes to cross the mid-transition point indicated that the X-ray suppression lags behind the optical rise by about half a day. This is an indication of the time the heating wave in the disc takes to propagate to the boundary layer. SS Cygni has also been observed to have a delay between optical and X-ray outbursts, with the beginning of X-ray outburst lagging behind the optical by 0.9 – 1.4 days (Wheatley et al. 2003). The shorter delay for SU UMa suggests that the time for the heating wave to travel through the disc is shorter, perhaps due to its smaller accretion disc.

The lack of an X-ray flux increase at the start of any of the outbursts is puzzling since the boundary layer is only thought to become optically thick once the accretion rate has reached a critical value (Pringle & Savonije 1979). In SS Cygni, the X-rays do increase before being suddenly suppressed (Wheatley et al. 2003). It may be that the quiescent accretion rate in SU UMa is already close to the critical rate. However, our estimated accretion rate in quiescence (4.2×10^{15} g s^{-1}) is below the expected critical value of 2×10^{16} g s^{-1}, although this does depend on the white dwarf mass and radius, the viscosity of the disc and temperature of the shocked gas (Pringle & Savonije 1979). In SS Cygni the transition is seen at an accretion rate of 1×10^{16} g s^{-1} (Wheatley et al. 2003). Alternatively, the observations presented here might have missed the flux increase. The optical rise in SS Cygni was approximately 1.5 days with an associated duration of 12 hours for the rise in the hard X-rays. The optical rise in SU UMa was approximately 1 day but the average separation of points in the composite light curve of Fig. 3 results in an upper limit of 2 hours to the duration of a peak that occurs at the same outburst phase and with the same duration in each case. An increase in flux was also not seen in VW Hyi

(Wheatley et al. 1996), although these observations had a cadence of one observation a day.

The X-ray suppression occurred very rapidly and is not resolved in our composite light curve, with a cadence of 2 hours (Fig. 4). This is similar to SS Cygni where the suppression occurred in less than 3 hours (Wheatley et al. 2003).

The X-ray recovery began while the optical band was in decline from outburst. This is earlier than seen in VW Hyi where the X-ray recovery occurred at the end of the optical outburst (Wheatley et al. 1996). Presumably this is due to a cooling front reaching the boundary layer before passing through the whole disc, perhaps suggesting that the cooling wave in SU UMa does not start at the outer edge of the disc.

The X-ray count rates measured for SU UMa tend to decrease during quiescence, dropping by 12 per cent over 8 days. This is also seen in SS Cygni by McGowan et al. (2004), where the decrease was by 40 per cent over 31 days. It is interesting to note that in both cases the count rate drops by about 1.7 per cent day^{-1}, perhaps indicating similar timescales acting in the inner accretion discs. The decrease in X-ray flux is in direct conflict with the disc instability model which predicts increasing quiescent accretion rates (e.g. Lasota 2001).

The X-ray spectrum of SU UMa in outburst is softer and fainter than during quiescence, in common with other dwarf novae (e.g. Baskill et al. 2005). The X-rays observed during quiescence arise from an optically thin region that is probably replaced by an unseen optically thick emitting region that most likely dominates during outburst. Spectral fitting of the data shows that a thermal plasma model with sub-solar abundances of 0.64 ± 0.01 and a 6.4 keV line describes the data well. The data are also consistent with the presence of a constant reflection continuum.

The luminosity during outburst, 7×10^{31} ergs s^{-1}, was similar to that calculated by Baskill et al. (2005) for SU UMa, with *ASCA*. Other systems observed by *ASCA* in outburst include RU Peg (9.4×10^{31} ergs s^{-1}), a U Gem system. During quiescence SU UMa had an average luminosity of $2.6 \times 10^{32}(d/260pc)^2$ ergs s^{-1}, about as luminous as SS Cygni (3.6×10^{32} ergs s^{-1}) but more luminous than U Gem (2.8×10^{31} ergs s^{-1}). T Leo, a SU UMa system, was also calculated to be less luminous with a luminosity of $1.8{\times}10^{31}$ ergs s^{-1}. The average luminosity during quiescence corresponds to a quiescent accretion rate of $4.2{\times}10^{15}$ g s^{-1}. This is similar to the quiescent rate of 3×10^{15} found by Wheatley et al. (2003) for SS Cygni and is two and a half orders of magnitude higher than predicted by the disc instability model (e.g. Hameury et al. 2000).

ACKNOWLEDGEMENTS

We thank D. Baskill for his role in planning the observations presented in this paper and the anonymous referee for constructive comments. This research has made use of data obtained through the High Energy Astrophysics Science Archive Research Centre Online Service, provided by the NASA/Goddard Space Flight Centre. We thank the *AAVSO* for providing optical light curves, which are based on observations by variable-star observers worldwide. DJC acknowledges funding from an STFC Studentship. Astrophysics research at the University of Warwick is funded by an STFC rolling grant.

REFERENCES

Anders E., Grevesse N., 1989, Geochim. Cosmochim. Acta, 53, 197
Baskill D. S., Wheatley P. J., Osborne J. P., 2005, MNRAS, 357, 626
Byckling K., Osborne J. P., Wheatley P. J., Wynn G. A., Beardmore A., Braito V., Mukai K., West R. G., 2009, ArXiv e-prints
Cordova F. A., Mason K. O., 1984, MNRAS, 206, 879
Eracleous M., Halpern J., Patterson J., 1991, ApJ, 382, 290
George I. M., Fabian A. C., 1991, MNRAS, 249, 352
Hameury J.-M., Lasota J.-P., Warner B., 2000, A&A, 353, 244
Jahoda K., Markwardt C. B., Radeva Y., Rots A. H., Stark M. J., Swank J. H., Strohmayer T. E., Zhang W., 2006, ApJS, 163, 401
Jones M. H., Watson M. G., 1992, MNRAS, 257, 633
Knigge C., 2006, MNRAS, 373, 484
Lasota J.-P., 2001, New Astronomy Review, 45, 449
Liedahl D. A., Osterheld A. L., Goldstein W. H., 1995, ApJ, 438, L115
Magdziarz P., Zdziarski A. A., 1995, MNRAS, 273, 837
McGowan K. E., Priedhorsky W. C., Trudolyubov S. P., 2004, ApJ, 601, 1100
Mewe R., Gronenschild E. H. B. M., van den Oord G. H. J., 1985, A&AP, 62, 197
Mewe R., Lemen J. R., van den Oord G. H. J., 1986, A&AP, 65, 511
Mukai K., Wood J. H., Naylor T., Schlegel E. M., Swank J. H., 1997, ApJ, 475, 812
Pandel D., Córdova F. A., Mason K. O., Priedhorsky W. C., 2005, ApJ, 626, 396
Patterson J., Raymond J. C., 1985, ApJ, 292, 550
Pringle J. E., 1977, MNRAS, 178, 195
Pringle J. E., Bateson F. M., Hassall B. J. M., Heise J., van der Woerd H., Holberg J. B., Polidan R. S., van Amerongen S., van Paradijs J., Verbunt F., 1987, MNRAS, 225, 73
Pringle J. E., Savonije G. J., 1979, MNRAS, 187, 777
Rana V. R., Singh K. P., Schlegel E. M., Barrett P. E., 2006, ApJ, 642, 1042
Ricketts M. J., King A. R., Raine D. J., 1979, MNRAS, 186, 233
Shakura N. I., Syunyaev R. A., 1973, A&A, 24, 337
Silber A., Vrtilek S. D., Raymond J. C., 1994, ApJ, 425, 829
Singh K. P., White N. E., Drake S. A., 1996, ApJ, 456, 766
Thorstensen J. R., 2003, AJ, 126, 3017
Tylenda R., 1981, Acta Astronomica, 31, 267
Verbunt F., Wheatley P. J., Mattei J. A., 1999, A&A, 346, 146
Warner B., 1995, Cataclysmic variable stars. Cambridge Astrophysics Series, Cambridge, New York: Cambridge University Press, —c1995
Wheatley P. J., Mauche C. W., 2005, in Hameury J.-M., Lasota J.-P., eds, The Astrophysics of Cataclysmic Variables and Related Objects Vol. 330 of Astronomical Society of the Pacific Conference Series, Chandra X-ray Observations of WZ Sge in Superoutburst. pp 257–+
Wheatley P. J., Mauche C. W., Mattei J. A., 2003, MNRAS, 345, 49
Wheatley P. J., Verbunt F., Belloni T., Watson M. G., Naylor T., Ishida M., Duck S. R., Pfeffermann E., 1996, A&A, 307, 137
Wheatley P. J., West R. G., 2003, MNRAS, 345, 1009
Wilms J., Nowak M. A., Dove J. B., Fender R. P., di Matteo T., 1999, ApJ, 522, 460
Wilms J., Nowak M. A., Pottschmidt K., Pooley G. G., Fritz S., 2006, A&A, 447, 245

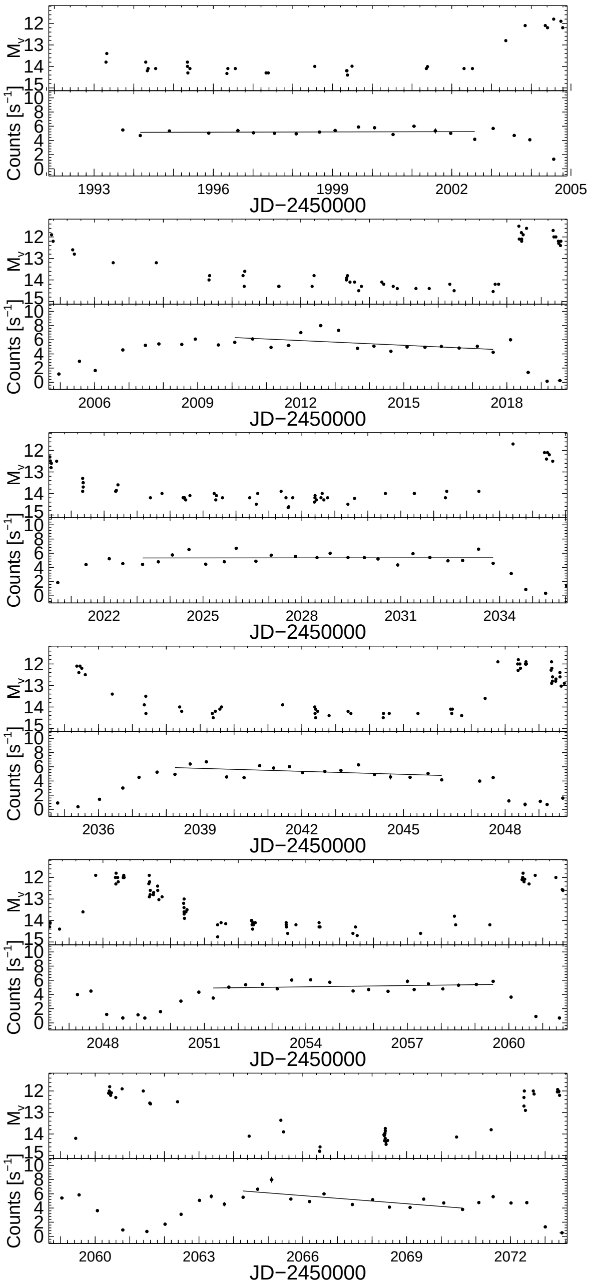

Figure 4. Individual optical (upper panel) and X-ray (bottom panel) light curves from Fig. 1 centred around the quiescent intervals. Each quiescent X-ray interval is also plotted with a linear least squares fit at times when the optical magnitude was fainter than 14^{th} mag. The X-ray count rates are for 3 *PCU*.

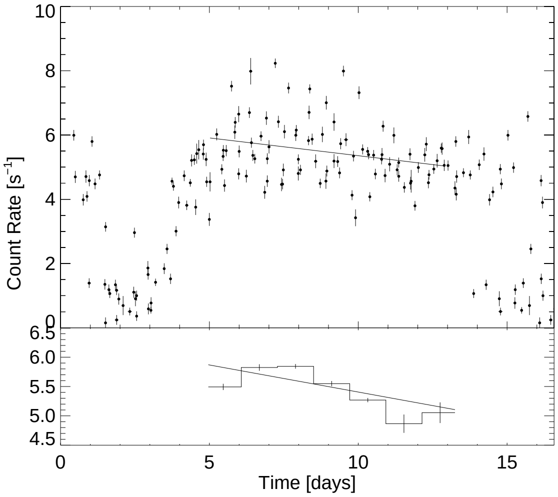

Figure 5. Composite X-ray light curve from Fig. 3 centred around the quiescent interval with a linear least squares fit to the quiescent data (top panel) and to the binned quiescent data (bottom panel) at times when the optical magnitude was fainter than 14^{th} mag. The X-ray count rates are for 3 *PCU*.

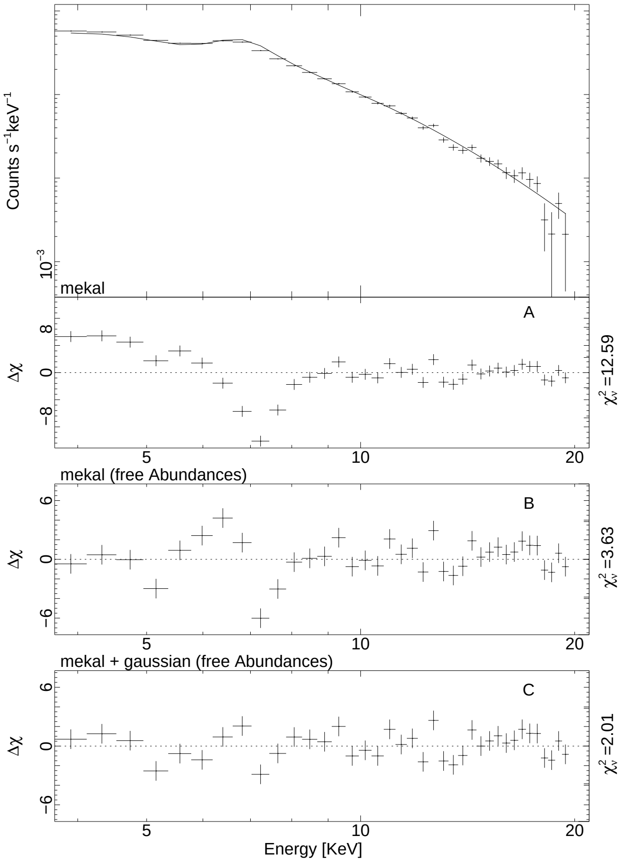

Figure 6. The top panel shows the data (crosses) and the folded model of a single temperature continuum model for the combined quiescence spectra (Section 4.1). The panels below show the residuals for this model and fits to subsequent models. The model, as used in `XSPEC`, is labelled above the residuals, with the χ^2_ν at the end of the individual panel. All errors are in the 68 per cent confidence interval for one parameter of interest ($\Delta\chi^2 = 1.0$)

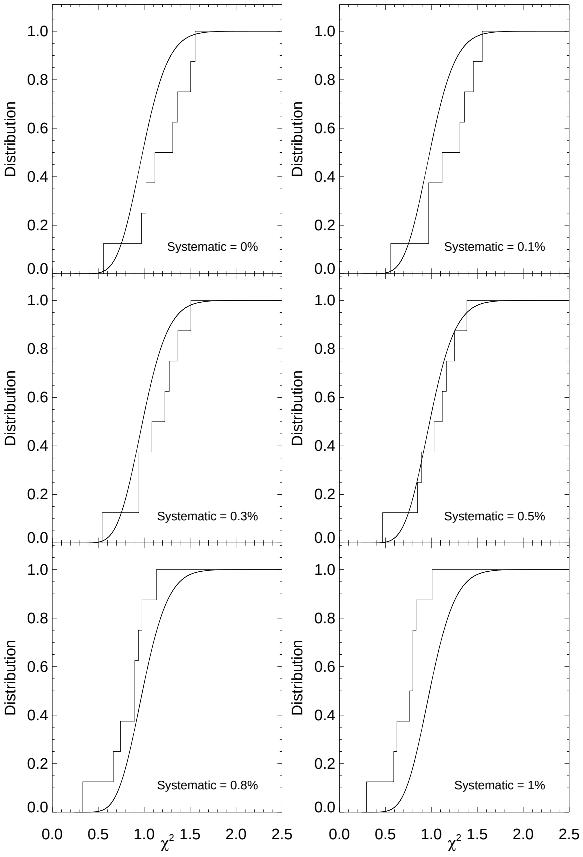

Figure 7. Cumulative histogram plots of χ^2_ν resulting from fits of all spectra to the thermal plasma model with a narrow emission line. The foreground systematic error is fixed at 0.5 for all fits while the background systematic is varied from 0 to 1 per cent.

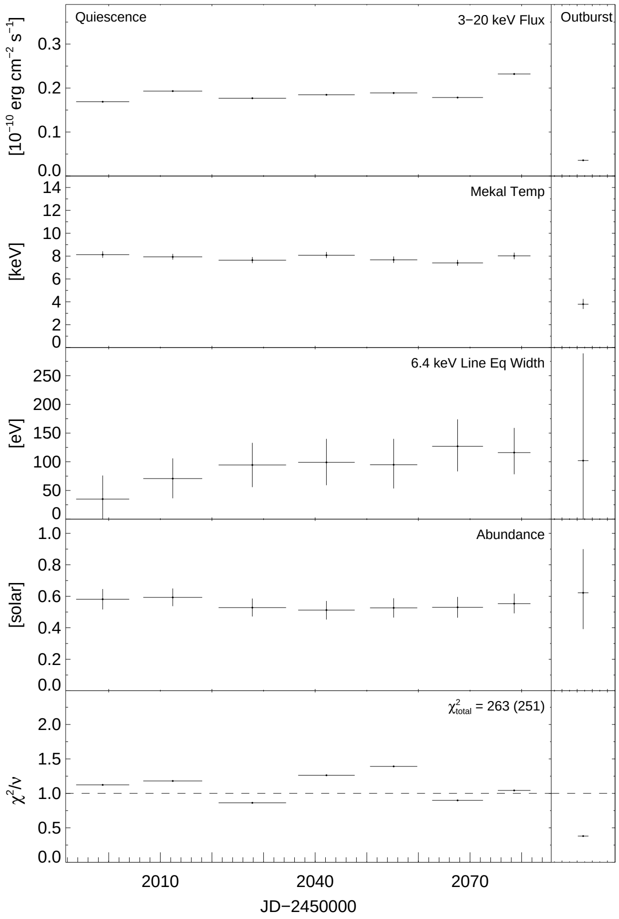

Figure 8. Thermal plasma model with the addition of a fixed 6.4 keV emission line component due to fluorescence. X-axis error bars mark the start of the first observation until the end of the last observation of the original spectra used to produce that spectrum. The spectra to the far right of the plot contains all outburst data and is thus plotted separately. All errors are in the 68 per cent confidence interval for one parameter of interest ($\Delta\chi^2 = 1.0$).

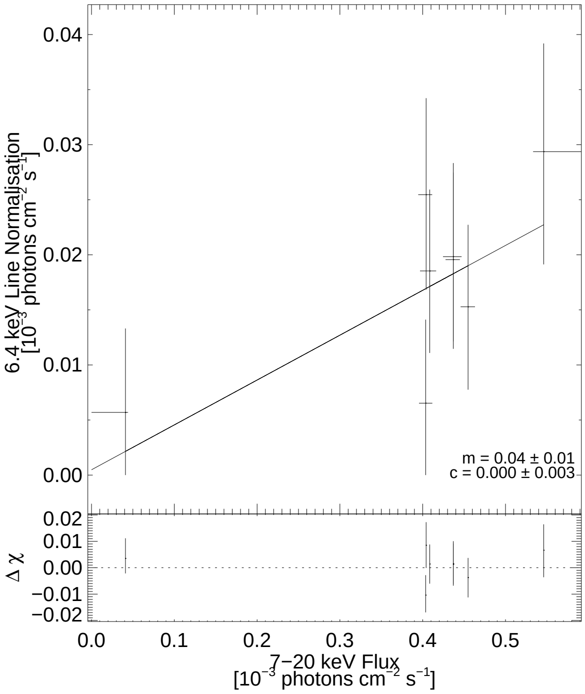

Figure 9. The best fit 6.4 keV line normalisation and the continuum flux above 7 keV. Also plotted is the best fit line to the data points. The bottom panel shows the residuals between the best fit line and the data. All errors are in the 68 per cent confidence interval for one parameter of interest ($\Delta\chi^2 = 1.0$).